X-ray diffraction analysis of the structure and residual stresses of W/Cu multilayers

Baptiste Girault, Pascale Villain, Éric Le Bourhis, Philippe Goudeau, Pierre-Olivier Renault

X-ray diffraction analysis of the structure and residual stresses of W/Cu multilayers

B. Girault, P. Villain, E. Le Bourhis, P. Goudeau, P.-O. Renault

University of Poitiers — Laboratoire de Métallurgie Physique, UMR 6630 CNRS, SP2MI, BD Marie et Pierre Curie, BP 30179, F-86962 Futuroscope Chasseneuil Cedex, France

A structural study has been carried out on tungsten layers from W/Cu multilayers (copper plays the role of spacer) prepared by ion beam sputtering. Using X-ray diffraction, three series of W/Cu multilayers were prepared, each one with various tungsten thicknesses (12, 3, 1.5 nm) but with constant nominal copper thickness (1, 0.5, 0 nm). X-ray diffraction measurements reveal that tungsten layers are systematically under strong compressive stress state. Thin film average stress values obtained using curvature method are compressive and lower than those determined from tungsten x-ray diffraction. All the multilayers showed stratification as revealed by X-ray reflectometry diagrams. It has been observed that samples with nominal copper thickness beneath 0.5 nm present two preferential crystallographic orientations: namely {110} and {111}. Moreover, all observed textures present a rotational isotropy in the sample surface plane (fiber-texture). An original {111} tungsten fiber-texture has been evidenced and its presence depends on the interface quality. A correlation between measured stresses, interface oxidation and preferential crystallographic orientations is suggested.

Keywords: X-ray diffraction; Tungsten; Multilayer; Sputtering; Interfaces; Texture

1. Introduction

Mechanical characteristics like residual stresses, hardness, elastic modulus and, interfacial adhesion are of great importance for advanced coating technologies [1]. X-ray diffraction is one of the most commonly used techniques to determine the residual stress state in small crystalline volumes [2,3]. It is phase selective and hence a unique technique that allows determination of both the mechanical and micro-structural states of the diffracting phases. Mechanical and X-ray elastic constants of thin films may differ from the bulk material counterparts. This difference is to be attributed to the unique nanostructure of thin films, the large surface to volume ratio, and the constraints caused by the supporting substrate [4–6]. Studying and tailoring the size effect on elastic constants of polycrystalline thin films require controlling the nanostructure (grain size, residual stresses, texture). One way to control grain size along one direction at nanometric scales is to prepare multilayers. However, regarding the system studied here, namely W/Cu multilayers, and in spite of the immiscibility of the two materials under condition of thermodynamic equilibrium, physical vapour deposition (PVD) may induce mixing effects. This effect results from the fact that PVD layers are out of equilibrium [7]. This has already been reported for multilayers with equal thickness of W and Cu [8]. In order to minimize this phenomenon, the approach proposed here is to decrease one material thickness i.e. copper thickness; from here onward, the Cu layer will be called the spacer. Nevertheless, we have to ensure that it does not affect the microstructure of the studied layers, i.e. tungsten layers. Moreover, because of the very small diffracting volumes and the need for quantitative strain measurements to study size effects on elastic constants, obtaining textured tungsten is an essential issue. Indeed, the more tungsten layers show preferential crystallographic orientations, the better diffraction peaks in pole directions are defined. The present paper reports on the evolution of the microstructure and texture in function of the thickness of the spacer and of the tungsten layers.

2. Experimental procedures

The W/Cu multilayer thin films were produced at room temperature by physical vapour deposition with an Ar^+-ion-gun

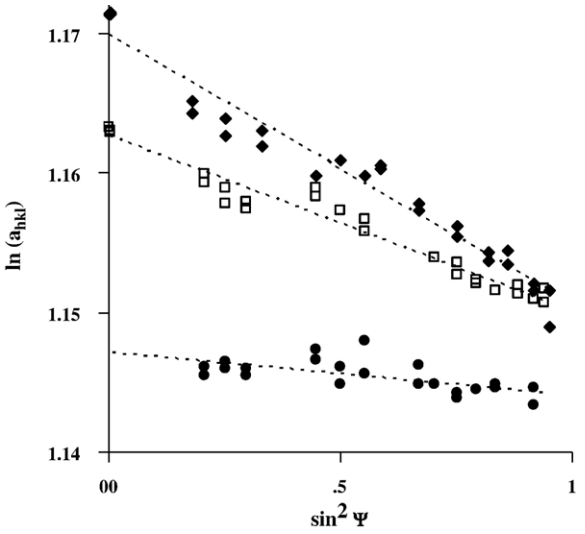

Fig. 1. $\mathrm{Sin}^2\psi$ plots and associated linear regressions (dashed lines) for sample series with a 1 nm copper nominal thickness value: (♦) t_W=12 nm, (□) t_W=3 nm and (●)t_W=1.5 nm. XRD measurements were performed on tungsten (110), (200) and (211) diffracting planes. The lattice parameter a_{hkl} is given in angströms.

sputtering beam at 1.2 keV in a NORDIKO-3000 system. The base pressure of the deposition chamber was 7×10^{-5} Pa while the working pressure during films growth was approximately 10^{-2} Pa. Two types of substrates were used: 200 and 650 μm thick naturally oxidized Si (001) wafers. The two deposition speeds used here were 0.5 Å s^{-1} for W and 1.6 Å s^{-1} for Cu. Phase analyses were performed on a SIEMENS D 5005 X-ray diffractometer (XRD) using Cu–K_α radiation in a θ–2θ geometry. Complementary XRD measurements were carried out on a four-circle goniometer (SEIFERT XRD 3000) using also the Cu–K_α radiation: the multilayers were examined by X-ray reflectometry to verify the existence of stratification and thus determine the period of each multilayer. High angle XRD was used to determine residual stresses in tungsten layers using the so-called "$sin^2\psi$ method". This method is based on the variation of the diffraction peak position with $\sin^2\psi$, ψ being the angle between the normal to the diffracting planes and the surface normal. In the case of an isotropic biaxial stress state, the "$\sin^2\psi$ relation" can be written as

$$\ln(a_{hkl,\psi}) = \frac{1+\upsilon}{E}\sigma\sin^2\psi - \frac{2\nu}{E}\sigma + \ln(a_0) \qquad (1)$$

where E and ν are the Young's modulus and the Poisson's ratio respectively.

Here the rational definition for strain $\varepsilon=\ln(a_{hkl}/a_0)$ is used, a_0 being the stress-free lattice parameter and a_{hkl}, the measured lattice parameter [9]. As a first approximation, tungsten bulk elastic constants (E=400 GPa and ν=0.28) were used. Diffraction peaks considered for this analysis have been measured in several pole directions. The expected linear behavior for isotropic tungsten is observed in Fig. 1 for three periods. Moreover, as the θ–2θ diagrams indicate preferential crystallographic orientations, rocking-curves were systematically recorded on tungsten (110) diffraction peak. Pole figures were also performed to get more precise information on the texture; they were made on tungsten (110), (200) and (211) peaks. Thin film residual stresses were determined using the curvature method with the multilayers deposited on 200-μm-thick Si cantilevers ($E/(1-\nu)$=180.5 GPa for Si (001) wafers). Several series of multilayers were prepared. Their nominal and effective thicknesses are listed in Table 1 as well as the different characteristics above mentioned. From here onward, the samples will be denominated using their nominal characteristics. Energy dispersive X-ray spectroscopy (EDXS) was used in the scanning electronic microscope (SEM) to determine atomic concentration of copper and tungsten elements in the films.

Table 1
Nominal and effective thicknesses of studied samples and associated measured stresses

Nominal thicknesses (nm)			Effective thicknesses (nm)			Total film thickness (nm)	Residual stresses (GPa)	
Λ	t_W	t_{Cu}	Λ	t_W	t_{Cu}		Film	W layers
3.0	3	0	2.8	2.8	0.0	180	−2.6	−4.3
12.5	12.0	0.5	11.0	10.8	0.2	170	−2.8	−5.3
3.5	3.0	0.5	3.0	2.8	0.2	200	−3.2	−5.8
2.0	1.5	0.5	1.7	1.5	0.2	180	−3.2	−6.8
13.0	12.0	1.0	10.9	10.0	0.9	180	−1.7	−6.2
4.0	3.0	1.0	3.3	2.7	0.6	200	−1.5	−4.0
2.5	1.5	1.0	2.1	1.5	0.6	220	0.0	−1.0

Λ and t correspond to the multilayer period and sub-layer (Cu and W) thicknesses respectively. Residual stresses in the film and W layers are determined by substrate curvature and XRD measurements respectively. Associated uncertainties are about 10%.

3. Results and discussion

As shown in Table 1, all thin film thicknesses are approximately 200 nm. Stress measurements reveal that all thin films

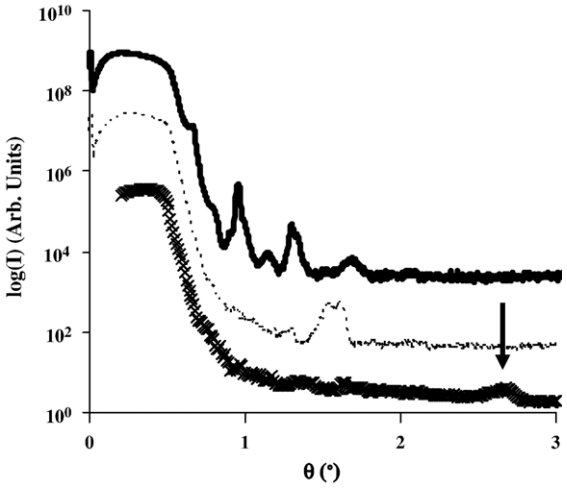

Fig. 2. X-ray reflectivity diagrams measured on sample series with a 0.5 nm constant copper nominal thickness: (—) t_W=12 nm, (---) t_W=3 nm and (xxx) t_W=1.5 nm. The arrow on the bottom curve indicates the position of the interference peak related to the modulation period for the smallest tungsten thickness.

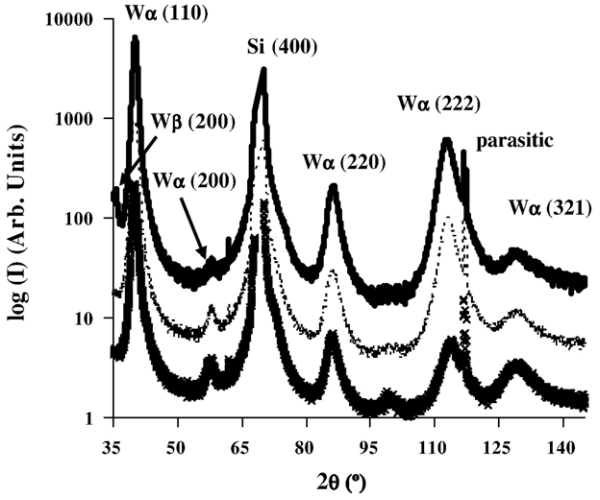

Fig. 3. Bragg–Brentano (θ–2θ) diagrams measured on sample series with a 0.5 nm constant copper nominal thickness: (—) t_W=12 nm, (---) t_W=3 nm and (xxx) t_W=1.5 nm.

are under compressive stress state. Tungsten layers present strong compressive stresses. It was not possible to determine stresses in copper sub-layers because of the too small available diffracting volumes. So far, it is important to note the significant difference between thin film average stresses and tungsten stresses for all samples. This difference attests that copper layers certainly present tensile stresses and thus may play an important role in the overall mechanical behavior. This effect may also be due to interface stress contribution and, in addition, to a residual stress overestimation in tungsten layers due to the use of bulk tungsten layer elastic constants [8]. The stress in tungsten layers is constant for the lower copper thickness whatever is the tungsten thickness while a decrease is observed in the case of thicker copper thickness when the tungsten thickness decreases. This last behavior is equivalent to the one observed in a previous study with equiatomic W/Cu multilayers [8].

It should be noticed that copper may represent less than two atomic layers in the case of 0.5 nm copper thickness series and one may wonder whether the films do present a multilayer type structure. Fig. 2 shows X-ray reflectivity diagrams for this series of samples. These diagrams do present Bragg's peaks attesting the existence of a modulation in all films, including the W1.5 nm/Cu0.5 nm multilayer. This result was unexpected since ion beam sputtering techniques are known to produce rough interfaces which effects are more important in the case of low periods. This last point may account for the sharp decrease of the reflected intensity observed in Fig. 2 beyond the flat plateau (total reflection). In addition, we can observe a decrease of the critical angle value θ_C with the period. This variation is related to the increase of copper contribution since the definition of θ_C is the following:

$$\theta_C = \sqrt{2\delta} \tag{2}$$

where δ (real part of the refractive index) is proportional to the film surface density.

It was impossible to obtain reliable simulations of the reflectivity diagrams. Indeed, roughness effects are very strong and thus difficult to evaluate properly. In a first approximation, we used the modified Bragg's law at small diffraction angles to determine the period of each multilayer:

$$2\Lambda\sin[\Theta(1-\delta/\sin^2\Theta)] = n\lambda \tag{3}$$

where Λ is the period, Θ the angular position of the nth multilayer Bragg's peak and λ the wavelength.

Experimental values reported in Table 1, are close to nominal ones within uncertainties.

Fig. 3 shows the θ–2θ diagrams performed on the same series of samples (0.5 nm Cu). No copper diffraction peaks are detected because of the low content of copper in the multilayers. The three multilayers present the body-centered cubic (BCC) a-phase of tungsten. Tungsten layers in this series present two preferential crystallographic orientations, namely {110} and {111}, the latter being evidenced by the strong (222) diffraction peak. However, regarding the W12 nm/Cu0.5 nm multilayer, the peak located at 2θ=35° indicates that this sample also presents a second phase of tungsten, the so-called β-phase (A15 structure). It is well known that this nonequilibrium phase is stabilized by the presence of oxygen atoms in interstitial sites of the cubic cell. Structural study of tungsten β-phase is difficult here due to the simultaneous presence of the a-phase. Indeed, β- and α-phases diffraction peaks localized around 2θ=40° are very close to each other and cannot be easily separated. The determination of {110} texture volumetric ratio is thus very difficult for samples presenting these two phases. It should be noted that the presence of β-phase does not prevent from studying the {111} texture of the a-phase since there is no β-W diffraction peaks in the relevant angular range. Then, we analyzed the evolution of the (222) diffraction peak as a function of tungsten period. Taking into account tungsten volumetric proportion, Fig. 3 reveals that increasing tungsten thickness reinforces {111} texture. The full widths at half maximum (FWHM) of the (110) and (222) diffraction peaks are almost constant when tungsten layer thickness

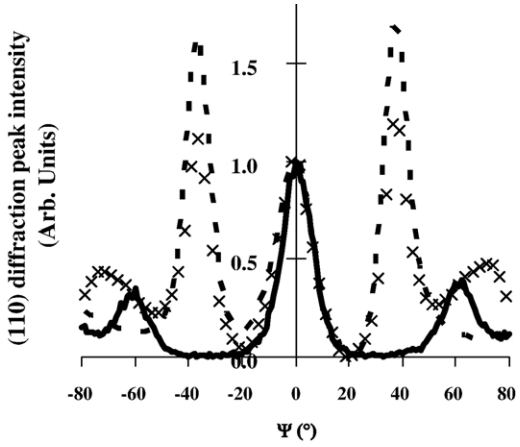

Fig. 4. Cross-sections of (110) tungsten pole figures measured on the three samples having the same 3 nm tungsten nominal thickness but different Cu thickness: (—) t_{Cu}=1 nm, (---) t_{Cu}=0.5 nm and (xxx) t_{Cu}=0.0 nm. The central peak intensity of the three curves has been normalized at 1.

decreases and are 1.2° and 3.6° respectively. Neglecting microstrains, the Scherrer formula [2,3] may be applied:

$$D = (0.9\lambda)/(\Delta 2\Theta \cos\Theta) \quad (4)$$

where $\Delta 2\Theta$ is the FWHM of the diffraction peak (in radian) and Θ is the angular diffraction peak position.

Calculation yields a grain size D along the growth direction of about 7.5 and 4.1 nm for <110> and <222> oriented grains respectively. These values are greater than the two smallest effective periods and then reveal the presence of partial coherency between layers at interfaces in these multilayers.

Several pole figures (not shown here) were recorded for the tungsten (110), (200) and (211) peaks for all samples to analyze the texture in tungsten layers. Fig. 4 presents radial cross-sections of the pole figures measured on the (110) α-W peak of 3 multilayers with constant W thickness (3.0 nm) and Cu thicknesses ranging from 0 to 1.0 nm. The intensity was normalized to the maximum intensity of the central peak. This figure is representative of the evolution of the texture with copper thickness. Looking at the sample having copper nominal thickness of 0.5 nm, we observe the existence of two components of texture. Indeed, the zero degree position peak clearly shows that classical {110} texture is present but the two peaks located at $\psi = \pm 35°$ (on both sides of the central peak) do not correspond to the angular values of pole directions expected between (110) planes but rather to those between (110) and (111) planes. This observation is confirmed by the results obtained for the two other pole figures. This implies that polycrystalline tungsten layers are made of a mixture of at least two sets of grains showing {110} and {111} preferred orientations. Finally, it appears that all tungsten layers of the 0.5 nm constant copper thickness sample series are {110} and {111} fiber-textured (figures not shown here).

The radial cross-section of the {110} pole figure of 3.0 nm thick tungsten layer recorded for the thicker copper interlayer (1.0 nm) shows three peaks located at $\psi = -60$, 0 and $+60°$ (Fig. 4). These angle values are characteristic of tungsten {110} texture, the classical texture found in BCC materials. This type of texture is observed on the three samples having a 1 nm copper nominal thickness value. Thus, it appears that increasing the copper nominal thickness from 0.5 up to 1.0 nm induces the loss of the {111} fiber-texture component.

These observations lead us to wonder what would happen when the copper thickness was decreased down to zero (no copper). The procedure used to prepare such a multilayer was nearly the same as the one used to produce the W3 nm/Cu0.5 nm multilayer, the target shutter being closed for 13 s (the sequence corresponding to copper deposition). This process is called "sequenced tungsten deposition". Unexpectedly, the X-ray reflectivity diagram (not shown here) of this sample shows a low angle diffraction Bragg's peak similar to the one obtained for the W3 nm/Cu0.5 nm multilayer in Fig. 2, which indicates the presence of a modulation period revealing the existence of a pseudo "interfacial layer". Hence we should consider this film as a multilayer W/-. More surprisingly, as observed in Fig. 4, tungsten layers in this sample do show the two fiber-texture components as already observed for the constant 0.5 nm copper nominal thickness samples series. The working pressure of the deposition chamber is relatively high (10^{-2} Pa) and may be involved in the existence of such an interfacial layer between each tungsten layer. Indeed, oxygen contamination may occur.

Several hypotheses may be suggested to explain such a texture evolution with copper thickness. First, it could be attributed to modifications of the deposition parameters used here. As reported in Ref. [10], texture is dependent on experimental deposition conditions (ion beam energy and flux, incident angle, deposition temperature…). However, all studied samples here were prepared using rigorously the same experimental conditions and thus this hypothesis does not support the tungsten texture evolution. Another explanation could involve the interface roughness of the copper intermediate layer. Indeed, 0.5 nm copper nominal thickness represents less than two average atomic layers (0.2 nm effective thickness). The Volmer–Weber growth mode certainly contributes to the existence of probably discontinuous and poorly-defined interfaces [11]. The large width and the weak intensity of the low angle Bragg's peaks shown on Fig. 2 confirm this point. The Bragg's peaks for W3 nm/Cu0.5 nm multilayer and W3 nm/-sequenced tungsten deposit are found to be similar. Moreover, the asymptotic intensity decreases after the critical angle indicates equivalent interfacial structure. These two samples yield the two texture components. This suggests that interfaces play an important role in the development of tungsten grains texture. For 1.0 nm copper layer thickness, we assume that copper layers are continuous as confirmed by X-ray reflectivity measurements (quality of the Bragg's peaks).

These results support the following hypothesis. Discontinuities at interfaces related to the low average copper layer thickness rule the presence of the tungsten {111} fiber-texture component as well as the presence of the β-W phase in tungsten layers. In view of results on new samples prepared by ion beam sputtering and also magnetron sputtering, we observe that β-W phase exists for all W/-samples prepared with different W thicknesses. When increasing the copper thickness up to 0.5 nm (nominal value), this phase remains only for the thicker tungsten layer (12 nm). It totally disappears for 1 nm copper nominal thickness. Undoubtedly, interfaces in sequenced W series are oxidized as well as the three samples prepared with 0.5 nm copper thickness, the copper certainly being oxidized. The presence of the two texture components is not dependent on the spacer nature, since both 0.5 nm copper thickness samples series and sequenced tungsten deposit present this particular texture. Graphs in Fig. 4 allow for a qualitative discussion on the evolution of the {111} texture between these two series. This figure clearly shows that tungsten {111} fiber-texture component in W3 nm/Cu0.5 nm multilayer is more important than the corresponding one in sequenced tungsten deposit.

The elastic energy related to residual stresses may also play an important role in the emergence of such a bimodal texture. However, since the tungsten is elastically isotropic, it may act in an equivalent way for the two components. So far, further knowledge on involved growth mechanisms is needed as well as observations of interfacial morphologies and in depth phase distribution in the film to determine whether tungsten grain growth is successively {111} textured and {110} texture, or two grain families having

only one preferential crystallographic orientation grow simultaneously and contribute to the final texture. Hence interface discontinuity has to be considered as well as interface oxidation. The interfacial layer may be a monolayer oxide that would modify the surface energy and thus the growing modes of tungsten layers. Chemical analyses at interfaces are then necessary.

4. Conclusion

Three series of W/Cu multilayers have been deposited by ion beam sputtering on (001) silicon wafers, each one with a different tungsten thickness (nominal values of 12, 3 and 1.5 nm) and a constant copper thickness (nominal values of 1, 0.5, 0 nm). As revealed by X-ray reflectivity and diffraction measurements, all these samples present a multilayered structure with {110} fiber-texture in tungsten layers. For a copper nominal thickness smaller than 0.5 nm, an additional {111} component of texture in tungsten layers is observed. To our knowledge, this is the first time that {111} fiber-texture is observed in tungsten thin films. The existence of two components of texture is ruled by the in-plane thickness homogeneity of the copper spacer layer and interface oxidation. The presence of β-W phase clearly indicates oxygen contamination of the film. The elastic energy related to thin film residual stresses is not a determinant parameter for the appearance of the two texture components since tungsten is elastically isotropic. Further experimental investigations are in progress such as quantitative texture measurements, cross-section transmission electron microscopy study of interfaces and in depth chemical analyses of the film.

Acknowledgments

The authors are gratefully indebted to Philippe Guerin at LMP for preparing the multilayered thin films. They would also like to thank N. Tamura (ALS, Berkeley) for thoroughly reading the manuscript and improving the English usage. This work has been granted by the French Agency for Research (ANR) through the Pnano project entitled Cmonano (ANR-05-PNANO-069).

References

[1] J.A. Thornton, J.E. Greene, in: R.F. Bunshah (Ed.), Handbook of Deposition Technologies for Films and Coatings, 2nd ed., Noyes, Park Ridge, NJ, 1994.

[2] I.C. Noyan, J.B. Cohen, Residual Stress Measurement by Diffraction and Interpretation, Springer, New York, 1987.

[3] V. Hauk, Structural and Residual Stress Analysis by Non Destructive Methods: Evaluation, Application, Assessment, Elsevier, Amsterdam, 1997.

[4] H. Huang, F. Spaepen, Acta Mater. 48 (2000) 3251.

[5] A.J. Kalkmann, A.H. Verbruggen, G.L.A.M. Jaussen, Appl. Phys. Lett. 78 (2001) 2673.

[6] J. Schiotz, T. Vegge, F.D. Di Tolle, K.M. Jacobsen, Phys. Rev., B 60 (1999) 11971.

[7] G. Ouyang, C.X. Wang, G.W. Yang, Appl. Phys. Lett. 86 (2005) 171914.

[8] P. Goudeau, P. Villain, T. Girardeau, P.-O. Renault, K.-F. Badawi, Scr. Mater. 50 (2004) 723.

[9] J. Lu, Handbook of Measurement of Residual Stresses, Society for Experimental Mechanics, Fairmont Press, Lilburn, GA, 1996.

[10] C.-H. Ma, J.-H. Huang, Haydn Chen, Thin Solid Films 446 (2004) 184.

[11] J.A. Floro, S.J. Hearne, J.A. Hunter, P. Kotule, E. Chason, S.C. Seel, C.V. Thompson, J. Appl. Phys. 89 (2001) 4886.